Reexamining the Moisture Mode Theories of the Madden–Julian Oscillation Based on Observational Analyses

FENG HU,[a] TIM LI,[b,a] JIANYUN GAO,[c] AND LISHENG HAO[d]

[a] *Key Laboratory of Meteorological Disaster, Ministry of Education/Joint International Research Laboratory of Climate and Environmental Change/Collaborative Innovation Center on Forecast and Evaluation of Meteorological Disasters, Nanjing University of Information Science and Technology, Nanjing, China*
[b] *Department of Atmospheric Sciences, School of Ocean and Earth Science and Technology, University of Hawai'i at Mānoa, Honolulu, Hawaii*
[c] *Fujian Key Laboratory of Severe Weather, Fujian Meteorological Bureau, China Meteorological Administration, Fuzhou, Fujian, China*
[d] *Tianjin Climate Center, Tianjin, China*

ABSTRACT: Two existing moisture mode theories of the MJO, one emphasizing boundary layer moisture asymmetry (MA) and the other emphasizing column-integrated moist static energy (MSE) tendency asymmetry (TA), were validated with the diagnosis of observational data during 1979–2012. A total of 2343 MJO days are selected. While all these days show a clear phase leading of the boundary layer moisture, 20% of these days do not show a positive column-integrated MSE tendency in front of MJO convection (non-TA). A further MSE budget analysis indicates that the difference between the non-TA composite and the TA composite lies in the zonal extent of anomalously vertical overturning circulation in front of the MJO convection. A background mean precipitation modulation mechanism is proposed to explain the distinctive circulation responses. Dependent on the MJO location, an anomalous Gill response to the heating is greatly modulated by the seasonal mean and ENSO induced precipitation fields. Despite the negative MSE tendency in front of MJO convection in the non-TA group, the system continues moving eastward due to the effect of the boundary layer moistening, which promotes a convectively unstable stratification ahead of MJO convection. The analysis result suggests that the first type of moisture mode theories, the moisture asymmetry mechanism, appears more robust, particularly over the eastern Maritime Continent and western Pacific.

KEYWORDS: Atmospheric circulation; Madden-Julian oscillation; Moisture/moisture budget

1. Introduction

The Madden–Julian oscillation (MJO) is the most prominent intraseasonal time scale mode in the tropics. It is characterized by slow eastward propagation (around $5 \, \text{m s}^{-1}$) along the equator over the Eastern Hemisphere (Madden and Julian 1972; Knutson 1986; Lau and Chan 1986; Hendon and Salby 1994; Lau and Lau 2010; Li and Hsu 2017; Jiang et al. 2020; Zhang et al. 2020) and at zonal planetary scale (Zhang 2005; Li and Zhou 2009; Li 2014). The discovery of this oscillation can be traced back to Madden and Julian (1971), or even earlier by Xie et al. (1963) [see Li et al. (2018) for a report on this earlier study]. The MJO is the major predictability source for seasonal to subseasonal forecast (Hsu et al. 2014; Xiang et al. 2015; Zhu et al. 2015). Therefore, it is critical to understand the basic propagation dynamics of the MJO.

A number of MJO theories have been developed during the past decades [see recent review papers by Zhang et al. (2020) and Jiang et al. (2020)]. Early theoretical studies regarded the MJO as a moist Kelvin wave modified by convective heating through a wave–CISK (conditional instability of the second kind) mechanism (e.g., Lau and Peng 1987; Chang and Lim 1988). But the so-derived mode had a too fast phase speed and favored the growth of shorter wavelengths, contrary to observed MJO characteristics. Emanuel (1987) put forward a wind-induced surface heat exchange (WISHE) mechanism, which relied on the existence of a mean easterly. However, in the most active MJO region (i.e., the Indo-Pacific warm pool), the pronounced mean wind is westerly (Wang 1988a). A convection–frictional convergence feedback (CFC) theory (Wang and Rui 1990; Wang and Li 1994; Li and Wang 1994) was proposed. It emphasized the coupling among free-atmospheric equatorial waves, boundary layer convergence, and convective heating. The heating was critical in forming a Kelvin–Rossby wave coupled structure (Wang and Li 1994; Hendon and Salby 1994). Without the longwave approximation in the meridional momentum equation, the model favored the growth of short waves under linear heating, and the planetary zonal scale was selected only when a nonlinear heating was specified (Li and Zhou 2009). A skeleton theory was proposed by Majda and Stechmann (2009). It emphasized the upscaling feedback of synoptic-scale and mesoscale convective systems to the MJO. An empirical relationship between the smaller-scale wave activity envelope and MJO-scale moisture was assumed (Thual et al. 2014; Thual and Majda 2015, 2016). Yang and Ingersoll (2013, 2014) put forward a gravity wave theory. The essence of this theory is the interference of westward and eastward inertia–gravity waves whose dispersion relations are not symmetric due to the beta effect. This theory, however, requires further observational validation.

Corresponding author: Tim Li, timli@hawaii.edu

One school of recent studies emphasized the important role of perturbation moisture in MJO propagation dynamics (e.g., Maloney 2009; Hsu and Li 2012; Sobel and Maloney 2012, 2013; Adames and Kim 2016; Kim and Maloney 2017; Maloney et al. 2019). The MJO moisture mode theories may be in general separated into two types (Wang and Li 2020a; Li et al. 2020). The first type emphasizes the zonal asymmetry of the perturbation moisture in the atmospheric planetary boundary layer (PBL) (Hsu and Li 2012). Hereafter we name this type as the boundary layer moisture asymmetry (MA) mechanism. The cause of the boundary layer moisture leading is primarily attributed to the advection of the mean moisture by anomalous ascending motion associated with the boundary layer convergence according to a moisture budget analysis, and the PBL convergence in front of MJO convection is a result of the MJO heating-induced Kelvin wave and a warm SST anomaly in front of MJO convection (Hsu and Li 2012). The boundary layer moistening in front of the convection gradually sets up local convective instability and triggers shallow and congestus convection, promoting the eastward propagation. The boundary layer moistening and congestus clouds developing processes were well documented by various observational studies (e.g., Johnson et al. 1999; Kikuchi and Takayabu 2004; Del Genio et al. 2012), including those during the DYNAMO observational campaign (Johnson and Ciesielski 2013). There was clearly stepwise progression from shallow cumulus to congestus and to deep convection. Wang et al. (2016) and Wang and Chen (2017) extended the previous CFC feedback model by including a perturbation moisture equation and applying a simplified Betts–Miller cumulus parameterization scheme in which precipitation depends on the perturbation moisture and a convective adjustment time. An MJO-like perturbation with a realistic eastward phase speed was simulated. The essential mechanism for the eastward propagation in the model lies in the PBL moisture leading. The PBL moisture-dependent parameterization scheme indirectly represents the congestus clouds development process, which has been emphasized in various theoretical models (e.g., Biello and Majda 2005; Khouider and Majda 2008).

The second type of the moisture mode theories emphasizes the zonal asymmetry of the column-integrated moisture or moist static energy (MSE) tendency, regardless of whether or not the PBL moisture is asymmetric. Hereafter we name the second type as the MSE tendency asymmetry (TA) mechanism. Sobel and Maloney (2012, 2013) first established a simple theoretical model using a column-integrated specific humidity tendency equation. The most unstable mode derived from the model had a too slow eastward phase speed compared to the observations. A detailed MSE budget analysis was conducted in a superparameterization general circulation model by Andersen and Kuang (2012), who pointed out the important role of the horizontal and vertical advection in promoting a zonally asymmetric MSE tendency. Adames and Kim (2016) improved the model framework by including anomalously meridional MSE advection proposed by Kim et al. (2014). Li and Hu (2019) further extended the theoretical framework by considering the advection of the mean MSE by anomalously second-baroclinic-mode vertical motion proposed by Wang

et al. (2017). The simple model was able to capture the planetary zonal-scale selection and slow eastward phase speed similar to the observations.

The moisture mode framework has been applied not only in theoretical and observational studies but also in the diagnosis of climate models. For instance, through diagnosing 27 global climate models that participated in a model intercomparison project organized by the MJO Task Force, Jiang et al. (2015) and Wang et al. (2017) revealed the fundamental dynamic processes responsible for the diverse simulations of MJO eastward propagation under the moisture mode framework. B. Wang et al. (2018) proposed a new MJO diagnosis matrix for diagnosing the climate model performance, which emphasizes the zonal asymmetry of MJO-scale circulation and moisture.

Given that the first and second types of the moisture mode theories emphasize different physical processes, one may wonder whether the two mechanisms operate simultaneously in all eastward-propagating MJO events, or on some days only one of the two mechanisms operates. Motivated by the aforementioned question, we intend to diagnose a large number of observed MJO days to investigate the relative importance of the two types of moisture mode dynamics in the eastward propagation. In particular, we will examine what percentage of the eastward propagating MJO days that involve only one of the two moisture mode mechanisms, and on these days what causes the eastward propagation.

The remaining part of this paper is organized as following. In section 2, data and methods are introduced. In section 3, moisture and MSE diagnoses for the all-days composite are discussed. Circulation characteristics of the non-TA group are introduced in section 4. Finally, conclusions and discussion are given in section 5.

2. Data and methods

a. Data

The primary datasets used in this study include satellite-measured daily outgoing longwave radiation (OLR) (Liebmann and Smith 1996) with a horizontal resolution of 2.5° × 2.5°, and daily averaged European Center for Medium-Range Weather Forecasts interim reanalysis (ERA-Interim; Dee et al. 2011) data. The reanalysis data consist of three-dimensional wind, geopotential height, temperature, specific humidity, and surface heat fluxes fields with a horizontal resolution of 1.5° × 1.5°. Fu et al. (2011) compared the MJO moisture fields in three reanalysis datasets (i.e., NCEP reanalysis I and II and ERA-Interim) with the direct satellite observations (TRMM). It was found that the quality of the humidity field was much better in ERA-Interim, which was used in the current study, than that in NCEP I and II. The current study focuses on a general boreal winter season (i.e., from 1 November to 30 April) in which eastward-propagating MJO signals are most pronounced. The analysis covers a 33-yr period (1979–2012).

b. Days selection

A real-time multivariate MJO (RMM) index (Wheeler and Hendon 2004) was used to select eastward propagating MJO

events. Before calculating the dominant EOF patterns of the OLR and upper and lower tropospheric zonal wind fields, a 20–100-day Lanczos bandpass filtering was applied to these fields. The leading EOF modes show strong MJO convective centers over the tropical eastern Indian Ocean and the western Pacific. Associated with the MJO convection is the low-level convergence and upper-level divergence, presenting a clear first-baroclinic-mode vertical structure. By reconstructing the OLR and wind data from the first and second EOF modes above, one may obtain the eastward propagating MJO signal. To remove some events with weak amplitude and short duration, we define the following criteria for the selection of MJO days: 1) the intensity of the OLR anomaly on a given day must be less than or equal to $-15\,\mathrm{W\,m}^{-2}$, 2) the MJO convection with the aforementioned daily OLR strength must be continually moving across 50° in longitude and must cross the eastern Indian Ocean (80°–100°E) and Maritime Continent, and 3) only MJO centers located between 60°E and 180° are considered.

With the criterion above, a total of 2343 MJO days were selected during the 33-yr period. Note that all selected MJO days propagate eastward. To describe the 3D circulation, moisture, and moist static energy fields associated with the eastward-propagating MJO signal, all fields are reconstructed based on the two leading principal components of the RMM index.

c. Rationale for separating two type moisture mode theories

Consider a simple scenario of a two-level free atmosphere on the equatorial beta plane without the PBL. Various free dry waves exist in a shallow water model, as demonstrated by Matsuno (1966). When considering an idealized circulation-dependent heating with prescribed background moisture distribution (e.g., Wang and Li 1994; Li and Zhou 2009), a similar set of wet wave solutions can be obtained, with a reduced gravity wave speed (due to the reduction of midtropospheric static stability). These wet waves are sometimes called as convectively coupled Kelvin, Rossby, mixed Rossby–gravity (MRG), and inertia–gravity (IG) waves. In the framework above, the governing equations are essential same as those in Matsuno (1966), and the perturbation moisture is not considered. With the inclusion of an additional prognostic moisture equation, a parameterization of diabatic heating in terms of the perturbation moisture is needed, in order to close the system. Currently the most popular way is to assume that the heating is proportional to the moisture (e.g., Wang et al. 2016; Wang and Chen 2017). With this parameterization and the two-level free atmospheric model, one would expect that the midtropospheric perturbation moisture is in phase with the anomalous ascending motion in situ, when a horizontally uniform background moisture is specified. Whereas such an in-phase relation may strengthen the perturbation and provide an additional instability, it does not contribute to phase propagation. An eastward phase propagation may occur when a positive moisture tendency appears in front of the convective center, for example, through the advection of a meridionally varying mean moisture by anomalous poleward flow caused by a negative heating anomaly in front of the convection (Kim et al. 2014). Such a scenario (i.e., the perturbation moisture remains symmetric while its tendency is asymmetric relative to the

convective center) is essentially same as the TA mechanism mentioned in the current study.

The scenario above is in great contrast with a situation in which the moisture itself is asymmetric. Note that the phase leading of the PBL moisture in front of the convection has been found by many previous observational studies (e.g., Sperber 2003; Hsu and Li 2012). The physical cause of this moisture asymmetry and its impact on the eastward propagation have been extensively studied (e.g., Hsu and Li 2012). A theoretical model based on this MA mechanism was constructed by Wang et al. (2016) and Wang and Chen (2017). Note that in this model the horizontal distribution of the background moisture was assumed to be uniform, which excluded the aforementioned meridional moisture advection effect. The heating in the model was proportional to column integrated moisture, which was the sum of free-atmospheric moisture and PBL moisture. While the former is in phase with the convection, the latter leads the convection due to the phase leading of Kelvin wave–induced PBL convergence. Thus, the PBL moisture leading provides a fundamental mechanism for eastward propagation in this simple theoretical model. It is worth mentioning that this perturbation moisture asymmetry mechanism differs from the previous PBL moisture convergence mechanism proposed by Wang and Rui (1990) and Wang and Li (1994) in which only the background mean moisture was considered.

In short, the MA and TA mechanisms have distinctive physical origins. The former emphasizes the asymmetry of the moisture itself, while the latter emphasizes the asymmetry of the column integrated moisture/MSE tendency. For the latter, the PBL process is not essential, as seen from the observed MSE budget analysis (Wang et al. 2017). The discussion above may help understand why the two distinctive moisture mode theories were proposed.

d. Moisture budget diagnosis

To understand specific processes that cause the PBL moisture leading, a moisture budget diagnosis was applied. Following Yanai et al. (1973), the moisture tendency equation on the intraseasonal time scale can be written as

$$\partial_t q' = -(\mathbf{V} \cdot \nabla q)' - (\omega \partial_p q)' - Q_2'/L, \tag{1}$$

where a prime denotes MJO-scale variables, q represents the specific humidity, $\mathbf{V}$ is the horizontal velocity, ∇ represents horizontal gradient, ω is vertical velocity, Q_2 is the apparent moisture sink, and L ($2.5 \times 10^6\,\mathrm{J\,kg}^{-1}$) is the latent heat of condensation. The first and second terms on the right-hand side (rhs) of Eq. (1) represent horizontal and vertical moisture advection, respectively. The third term denotes the moisture changing rate due to condensational heating.

A vertical average operator from 1000 to 700 hPa was applied to the moisture tendency equation to diagnose the relative contribution of each term on the rhs of Eq. (1) to the PBL moistening. Through this diagnosis, one may reveal specific physical processes responsible for the MA and the eastward propagation.

e. MSE budget diagnosis

To reveal the specific physical processes for the TA, we conduct a MSE budget diagnosis. MSE is defined as
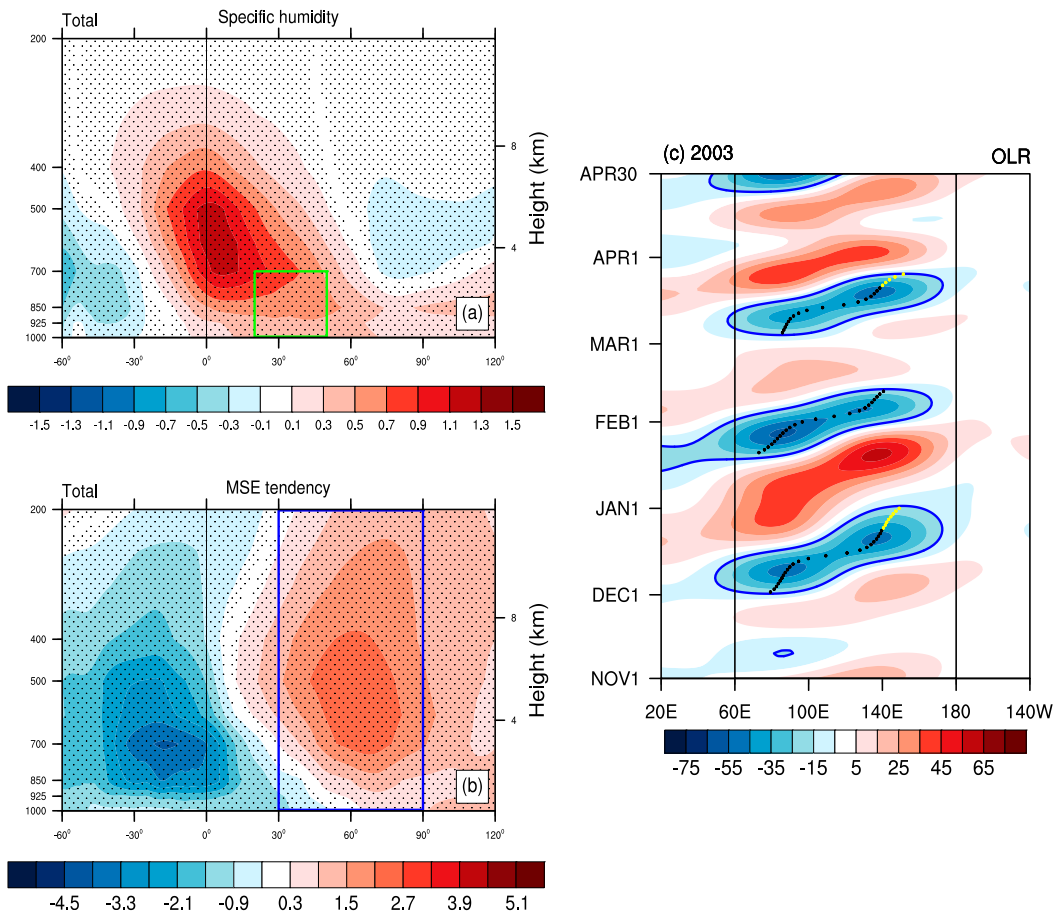
FIG. 1. Vertical–zonal cross section of (a) anomalous specific humidity ($g\,kg^{-1}$) and (b) MSE tendency ($10^{-3}\,m^2\,s^{-3}$) based on the total MJO days (2343 days) composite, averaged over $-10°$ and $10°$ to the center of MJO convection. Black lines represent the MJO convective center. The green box represents the PBL specific humidity leading region. The blue box denotes the positive MSE tendency leading region. The x axis represents the relative longitude distance to the MJO convective center. Dotted areas exceed a 95% confident level with Student's t test. (c) Hovmöller diagram of reconstructed OLR ($W\,m^{-2}$) averaged between 10°S and 10°N for the 2003/04 boreal winter. The blue contours indicate $-15\,W\,m^{-2}$ contours. Dots indicate the reference days for the selected events. Yellow dots represent days belong to the non-TA group. The longitude range under consideration is outlined in black lines.

$m = C_pT + gz + Lq$, where T is temperature, z is height, q is specific humidity, C_p ($1004\,J\,K^{-1}\,kg^{-1}$) is the specific heat at constant pressure, and g ($9.8\,m\,s^{-2}$) is gravity acceleration. Following Neelin and Held (1987), the column-integrated MSE budget equation on the MJO time scale may be written as

$$\langle\partial_t m\rangle' = -\langle \mathbf{V} \cdot \nabla m\rangle' - \langle\omega\partial_p m\rangle' + Q'_R + Q'_t, \qquad (2)$$

where angle brackets denote mass-weighted vertical integral from the surface to the tropopause. The first and second terms on the rhs of Eq. (2) represent, respectively, horizontal and vertical MSE advection, the third term denotes the sum of vertically integrated shortwave and longwave radiative heating rate, and the fourth term represents the surface latent and sensible heat fluxes.

Given that MSE is a conservative quantity in the tropics in the absence of diabatic processes (Neelin and Held 1987) and

that on the intraseasonal time scale, the MSE anomaly is in phase with the precipitation anomaly (Andersen and Kuang 2012). The MSE budget equation can be used to understand specific physical processes that give rise to the TA and thus eastward propagation.

3. Moisture and MSE budget diagnoses for the all-day composite

Figure 1a shows the composite pattern of anomalous specific humidity based on all the selected MJO days (i.e., a total of 2343 days). It can be seen that the specific humidity anomaly in the middle troposphere is in phase with MJO convection, while in the lower troposphere a positive moisture anomaly leads the MJO convection. Such an asymmetric structure matches well with the first type of the moisture mode theories, the MA mechanism.
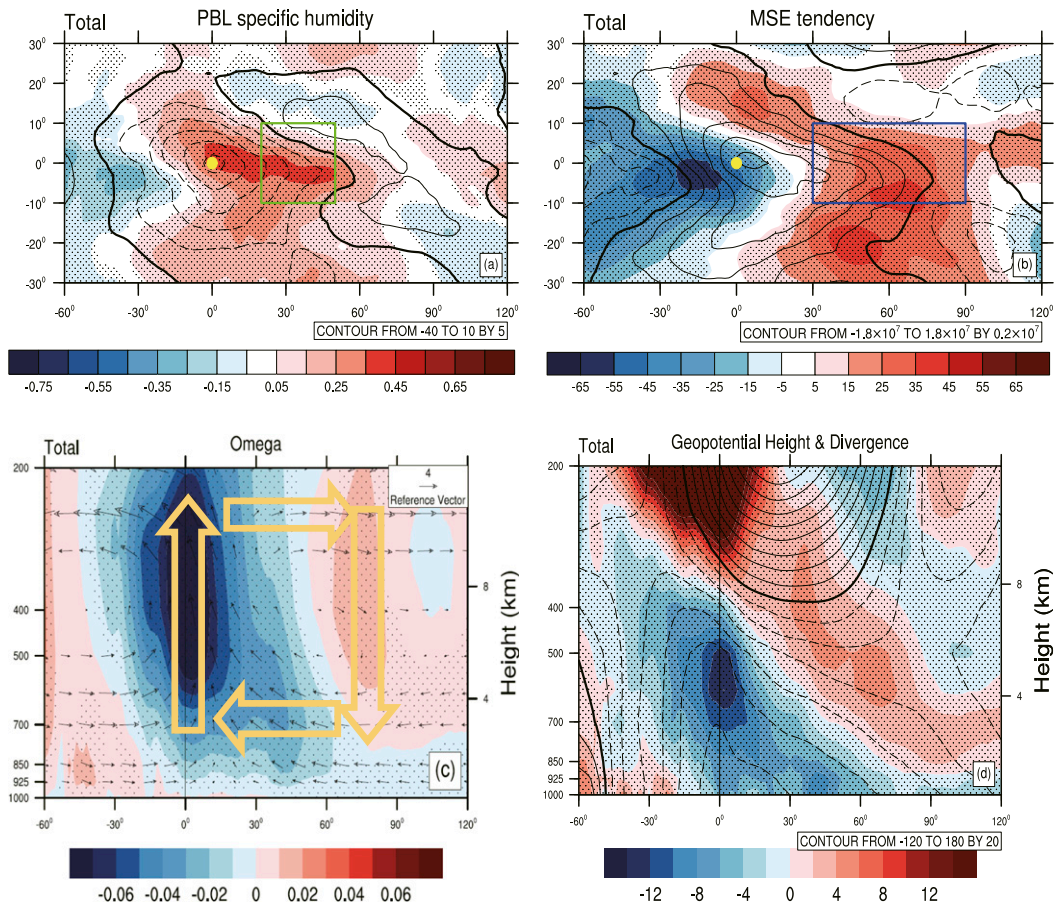
FIG. 2. (a) Horizontal composite patterns of anomalous PBL specific humidity (shaded; g kg^{-1}) and OLR (contours; W m^{-2}). (b) Horizontal composite patterns of anomalously column-integrated MSE tendency (shaded; kg s^{-3}) and MSE (contours; m^2 s^{-2}). Yellow dots represent the MJO convective center. Green and blue boxes represent, respectively, the key region for moisture and MSE tendency leading. The x (y) axis represents the relative longitude (latitude) distance to the center. (c) Vertical–zonal cross section of anomalous vertical velocity (shaded; Pa s^{-1}) and zonal and vertical velocity fields (vectors; m s^{-1} for zonal wind and 0.02 Pa s^{-1} for vertical pressure velocity). Yellow hollow arrows denote the vertical overturning circulation. (d) Vertical–zonal cross section of anomalous divergence (shaded; 10^{-7} s^{-1}) and geopotential height (contours; m^2 s^{-2}). Black lines represent the MJO convective center. All the panels are based on the total MJO days (2343 days) composite, averaged over $-10°$ and $10°$ to the center of MJO convection. Areas with dots exceed a 95% confident level with Student's t test.

Figure 1b shows the vertical profile of the anomalous MSE tendency derived from the all-day composite. Clearly it illustrates an east–west asymmetry, with a positive tendency to the east and a negative tendency to the west of MJO convective center. Such a zonal asymmetry of the MSE tendency is in agreement with the TA mechanism and promotes the eastward propagation of the MJO.

The horizontal view of the MA and the TA can be seen from the top panel of Fig. 2. Relative to the MJO convective center, a positive PBL moisture anomaly appears to its east (Fig. 2a), while a positive MSE tendency appears to the east and a negative MSE tendency appears to the west of the MJO center (Fig. 2b). The MJO convective center denotes the longitude where the minimum meridionally averaged (10°S–10°N) OLR appears.

The anomalous vertical velocity field shows a vertical tilting structure. While the midtropospheric ascending motion is in phase with the MJO convective center, the upward motion leads the convective center in the PBL and lags the convective center in the upper troposphere (Fig. 2c). The ascent at the upper troposphere to the rear of MJO is consistent with the characters of stratiform clouds, which has been emphasized to be important for MSE tendency asymmetry and MJO eastward propagation (Wang et al. 2017; Li and Hu 2019). The zonal width of Gill-type anomalous vertical overturning circulation is about 70° in longitude, as indicated by the yellow arrow in Fig. 2c. Over the MJO convective center, the free-atmospheric circulation is characterized by the first-baroclinic-mode structure, with a convergence in the lower troposphere and divergence in the upper troposphere. Away from the convective
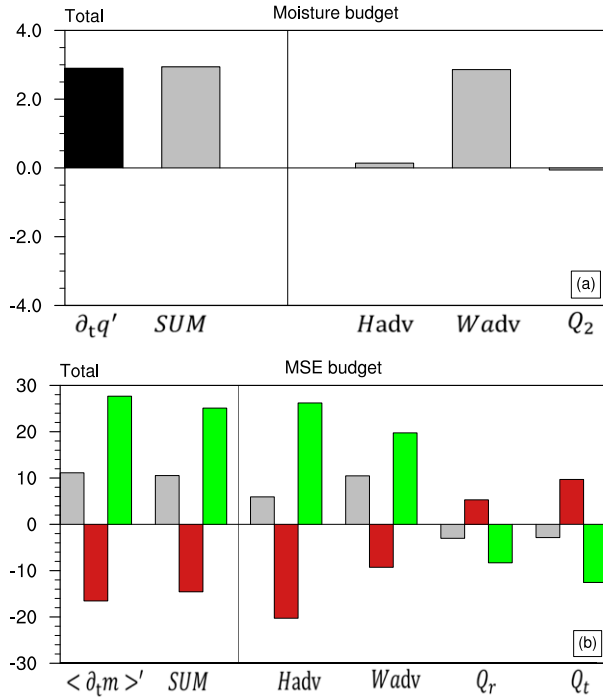
FIG. 3. (a) Vertically averaged (1000–700 hPa) moisture budget terms $(10^{-7}\,\mathrm{kg\,m^{-2}\,s^{-1}})$ averaged over the moisture leading region (20°–50°, from −10° to 10°; the green box in Fig. 1a). Bars from left to right represent, respectively, the observed specific humidity tendency, sum of budget terms, horizontal advection, vertical advection, and condensational heating rate. (b) Column-integrated MSE budget terms $(\mathrm{kg\,s^{-3}})$. Bars grouped from left to right represent, respectively, the MSE tendency, sum of budget terms, horizontal advection, vertical advection, radiation heating rate, and surface latent heat flux. Gray, brick red, and green bars represent, respectively, an average over the east box (30°–90°, from −10° to –10°; blue box in Fig. 1b), the west box (−50°–10°, from −10° to –10°), and the east–west box difference.

center, a second-baroclinic-mode structure exists, with a convergence in the lower and upper level and a divergence in the middle level east of the MJO convection (Fig. 2d). An opposite pattern appears to the west.

One question related to the MA mechanism is what causes the boundary layer moistening in front of the MJO convection. To answer the question, a vertically averaged (1000–700 hPa) moisture budget analysis is conducted over a key analysis region (i.e., the green box in Fig. 1a; hereafter this green box will be used to assess the MA mechanism). Figure 3a shows the budget analysis result. The largest contribution arises from the vertical advection term. To reveal specific processes responsible, the vertical advection term is further separated into three components as follows:

$$-(\omega\partial_p q)' = -\overline{\omega}\partial_p q' - \omega'\partial_p \overline{q} - \omega'\partial_p q', \qquad (3)$$

where a prime denotes intraseasonal time scale variable and a bar represents the background mean state. The diagnosis result shows that the dominant term is $-\omega'\partial_p \overline{q}$ (i.e., advection of the
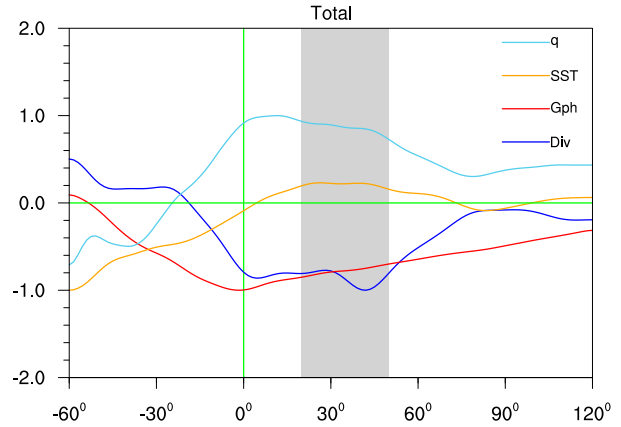
mean moisture by anomalous ascending motion; figures not shown). Because the mean moisture decays exponentially with height, the generation of anomalous ascending motion at the PBL holds a key.

What causes the anomalous low-level ascending motion in front of the MJO convection? According to Hsu and Li (2012), the anomalous ascent results from both the heating-induced free-atmospheric Kelvin wave response and an anomalous warm SST due to air–sea interaction. As seen from Fig. 4, a positive low-level moisture anomaly is approximately in phase with a low pressure anomaly at 700 hPa and a warm SST anomaly. The low pressure anomaly at the top of PBL may induce a boundary layer convergence and upward motion in situ, according to the Ekman pumping mechanism (Wang 1988b; Wang and Li 1993). A warm SST anomaly induced by reduced surface evaporation may cause boundary layer convergence and ascending motion through a pressure gradient force (Lindzen and Nigam 1987).

A key issue related to the TA mechanism is what causes a positive MSE tendency to the east of the MJO convection. Our MSE budget analysis shows that the key contribution arises from both horizontal and vertical MSE advection, while radiation and surface heat flux terms play a negative role (Fig. 3b). To isolate specific advective processes, we separated the horizontal and vertical MSE advection terms into linear and nonlinear advection terms as following:

$$
\begin{aligned}
-\langle \mathbf{V}\cdot\nabla m\rangle' - \langle \omega\partial_p m\rangle' = & -\langle \overline{u}\partial_x m'\rangle - \langle u'\partial_x \overline{m}\rangle - \langle u'\partial_x m'\rangle \\
& -\langle \overline{v}\partial_y m'\rangle - \langle v'\partial_y \overline{m}\rangle - \langle v'\partial_y m'\rangle \\
& -\langle \overline{\omega}\partial_p m'\rangle - \langle \omega'\partial_p \overline{m}\rangle - \langle \omega'\partial_p m'\rangle.
\end{aligned}
\qquad (4)
$$

The diagnosis result shows that the anomalous horizontal and vertical MSE advection terms are mainly attributed to the advection of the mean MSE by anomalous horizontal and
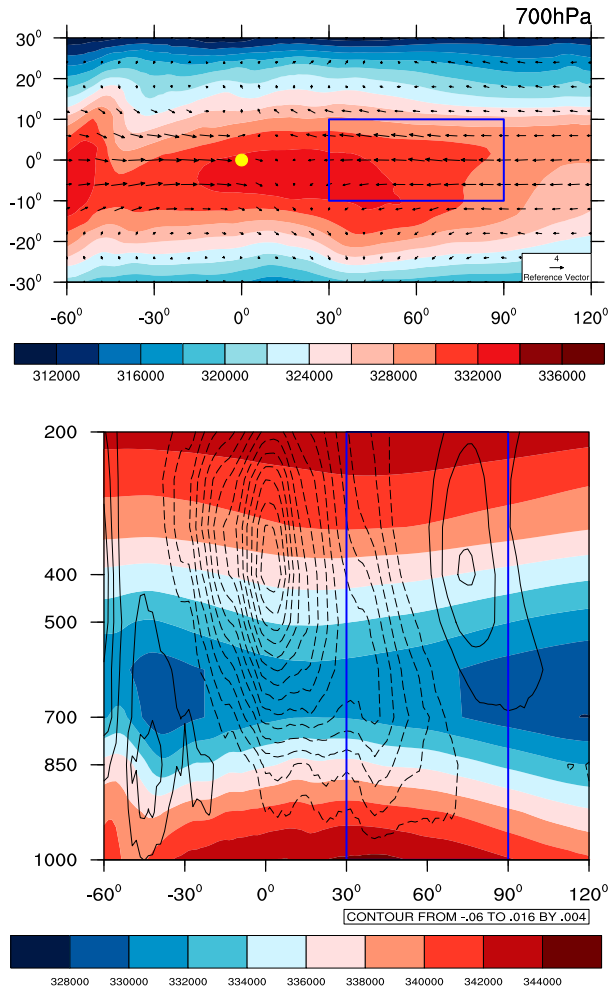
FIG. 5. (top) Composite patterns of anomalously horizontal wind (vectors; m s^{-1}) and mean MSE (shaded; m^2 s^{-2}) fields at 700 hPa. The yellow dot represents the MJO convective center. (bottom) Vertical–zonal cross section of anomalously vertical velocity (contours; Pa s^{-1}) and mean MSE (shaded; m^2 s^{-2}) field. Blue boxes represent the key regions. All fields are based on the total MJO composite.

vertical wind. While the maximum horizontal advection appears in the lower troposphere (near 700 hPa), the maximum vertical advection occurs in the upper troposphere (near 300 hPa) (figures not shown). The result is in good agreement with previous results (e.g., Wang et al. 2017; Wang and Li 2020b).

The cause of positive horizontal and vertical advection anomalies to the east of the MJO convection can be inferred from the mean MSE and the anomalous horizontal and vertical wind patterns shown in Fig. 5. The anomalous horizontal wind at 700 hPa is characterized by a modified Kelvin wave response to the east of the MJO main convection and a pair of Rossby wave gyre to the west (Li 2014). The poleward flow to the east is the part of Rossby wave response to the suppressed convection anomaly to the east of the MJO main convective center

(Wang et al. 2017; L. Wang et al. 2018). Given the maximum mean MSE near the equator, a poleward flow anomaly causes a positive MSE tendency to the east of the MJO convection.

The zonal–vertical section of Fig. 5b shows a descent (ascent) anomaly in the upper-middle (lower) troposphere to the east of the MJO convection. This anomalous vertical velocity acts on the mean MSE vertical profile (with a maximum near the tropopause and the surface and a minimum near 600 hPa) and causes a positive MSE tendency in situ. The result is again consistent with previous studies (e.g., Wang et al. 2017). It is worth mentioning that the positive vertical advection is primarily attributed to the upper-level part due to stronger intensities in both the mean MSE gradient and anomalous descent there. It is attributed to the advection of potential energy (gz) rather than moist enthalpy ($C_pT + Lq$). This highlights a critical difference of physical process operating in the MA and TA mechanisms.

To sum up, the diagnosis of the total-day composite above shows that both the MA and TA mechanisms are valid and important for promoting the eastward propagation of the MJO. What happened to individual MJO days? Will the two types of the moisture mode theories work for each of the individual days? To address the questions above, we develop a strategy to examine each of individual MJO days. For the MA mechanism, a PBL moisture index is introduced as the averaged moisture anomaly over the key region (the green box shown in Fig. 1a; 1000–700 hPa, from −10° to 10° and 20°–50°). By examining the moisture index in each day, one may estimate how many percentages of the MJO days satisfy the MA mechanism. A positive index implies that a positive moisture anomaly at the PBL leads to the MJO convection. Similarly, a TA index is introduced. It is defined as the column-integrated MSE tendency averaged over the domain of 1000–200 hPa, from −10° to 10° and 30°–90° as shown in the blue box of Fig. 1b (hereafter this blue box is used to assess the TA mechanism). A positive TA index implies that a positive column-integrated MSE tendency leads the MJO convection. It is worth mentioning that the blue box is located near the 90° phase of zonal profile of the column integrated MSE anomaly, implying that the TA index averaged over the domain links well to phase propagation. By examining this index at each of individual days, one may estimate the percentage of the MJO days that satisfy the TA mechanism.

It is found that a positive MA index appears in all the 2343 days. This suggests that the MA appears in all the days studied. However, 461 days (about 20% of the total days) possess a negative TA index, implying that during these days the MSE tendency asymmetry is not clearly presented. Note that all these special 20% days occur when the MJO center is located east of 140°E (hereafter these special days are referred to as the non-TA group).

The statistical analysis above indicates that for MJOs over the tropical Indian Ocean and western Maritime Continent (west of 140°E; 1745 days), both types of moisture mode theories are valid and can explain the MJO eastward propagation. When the MJO convective center passes 140°E, the MA mechanism still works, while the TA mechanism works only for about 23% of 598 days. In the next section, we will pay special

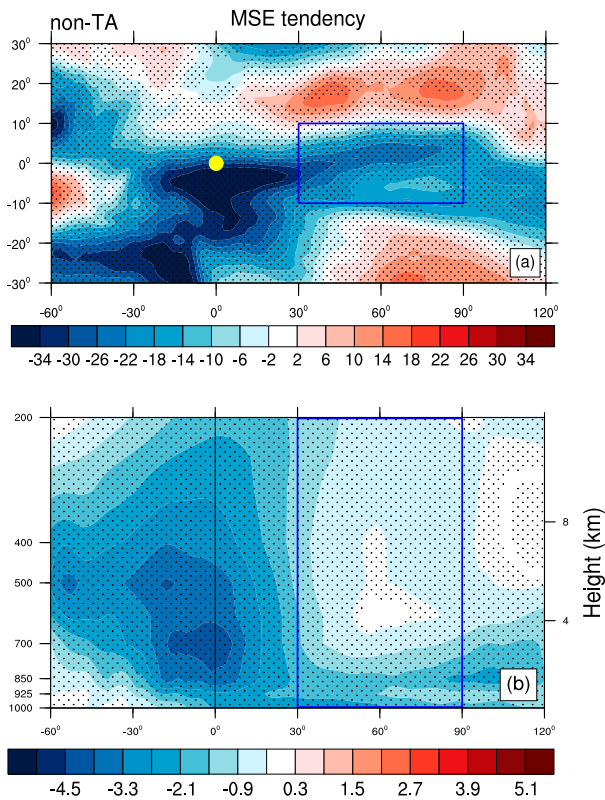FIG. 6. (a) Horizontal composite pattern (kg s^{-3}) and (b) vertical–zonal cross section (10^{-3} m^2 s^{-3}) of anomalous MSE tendency based on non-TA composite. The yellow dot and black line represent the MJO convective center. Blue boxes represent the tendency leading region. Areas with dots exceed a 95% confident level with Student's t test.

attention to the special non-TA group in order to understand the cause of the invalidation of the TA mechanism while the MA mechanism still operates.

4. Circulation characteristics and budget diagnoses of the non-TA group

Figure 6 shows the horizontal and vertical structure of the anomalous MSE tendency in the non-TA group composite. A clearly negative MSE tendency occurs to the east of the MJO convective center, which is at odds with the TA mechanism. A negative tendency also appears to the west of and near the MJO center, which implies an overall weakening of MJO strength during the period. Note that all the non-TA days are located east of 140°E, where the mean state and surface conditions may hinder the MJO development. Even though the TA mechanism does not work well in these non-TA days, MJOs still propagate eastward. This motivated us to further examine the MA mechanism.

Compared to the all-day composite, a similar phase leading of a positive PBL moisture occurs to the east of the MJO convection in the non-TA group (Fig. 7a). An important difference is the absence of anomalous descent over the key

region for TA (30°–90° east of the MJO convective center) (Fig. 7b). A weak descent anomaly occurs farther to the east (east of 120°), which connects to the low-level easterly anomaly, forming a zonally extended anomalous vertical overturning circulation (Gill 1980). This zonally expended Kelvin wave response is consistent with the first baroclinic mode structure of the geopotential height field in the free atmosphere, with a negative (positive) anomaly in the lower (upper) troposphere (Fig. 7c). In response to the anomalous low pressure forcing at the top of the PBL, area-averaged boundary layer convergence and ascending motion appear to the east of the MJO center (Figs. 7b,c).

A column-integrated MSE budget analysis is conducted to reveal the cause of the negative MSE tendency in the blue box region. The contribution for each term is shown in Fig. 8a. The horizontal advection term is positive, while the vertical advection and surface heat flux terms are negative. The sum of these terms makes a negative MSE tendency anomaly east of the MJO convection. Compared to the all-day composite (Fig. 3b), the most important difference appears in the vertical advection term (Fig. 8b).

By comparing the decomposed vertical advection fields in the non-TA and the all-day composites, one may find that the difference is primarily attributed to the advection of the mean MSE by anomalous vertical velocity in the upper-middle troposphere. The anomalous vertical velocity and the mean MSE distributions in the non-TA group are shown in Fig. 8c. Consistent with Fig. 7b, upward vertical motion anomalies dominate the upper-middle troposphere over the key analysis region. The anomalous ascent leads to the column-integrated negative MSE tendency (due to the advection of the potential energy) in the non-TA group. Despite the upper-level negative MSE tendency, low-level moistening process still happens in front of the MJO convection. This unveils a fundamental difference in the MA and TA mechanism.

What causes an obvious descent east of MJO convection (at 30°–90°) in the all-day composite but not in the non-TA composite? We hypothesize that it is attributed to the zonal distribution of the background (including the mean and interannual) state. The top panel of Fig. 9 illustrates the climatological boreal winter mean SST, precipitation, and low-level specific humidity fields, whereas the lower panels of Fig. 9 show the interannual counterparts for the following three groups: 1) all MJO days west of 140°E (1745 days), 2) MJO days east of 140°E that belong to the TA group (137 days), and 3) MJO days east of 140°E that belong to the non-TA group (461 days). For group 1, the composite MJO center is located at 95°E, and there is pronounced seasonal mean precipitation to the date line. Because the associated interannual SST and precipitation anomalies in the Pacific are weak, the background state is primarily controlled by the mean state. For groups 2 and 3, the MJO center is located at 150°E. The background SST and precipitation are modulated by the interannual counterparts. In group 2, an El Niño–like SST pattern with positive rainfall and moisture anomalies appears to the central and eastern Pacific. This extends the background mean precipitation eastward. In contrast, a La Niña–like SST pattern with suppressed rainfall and a negative specific humidity anomaly appears in
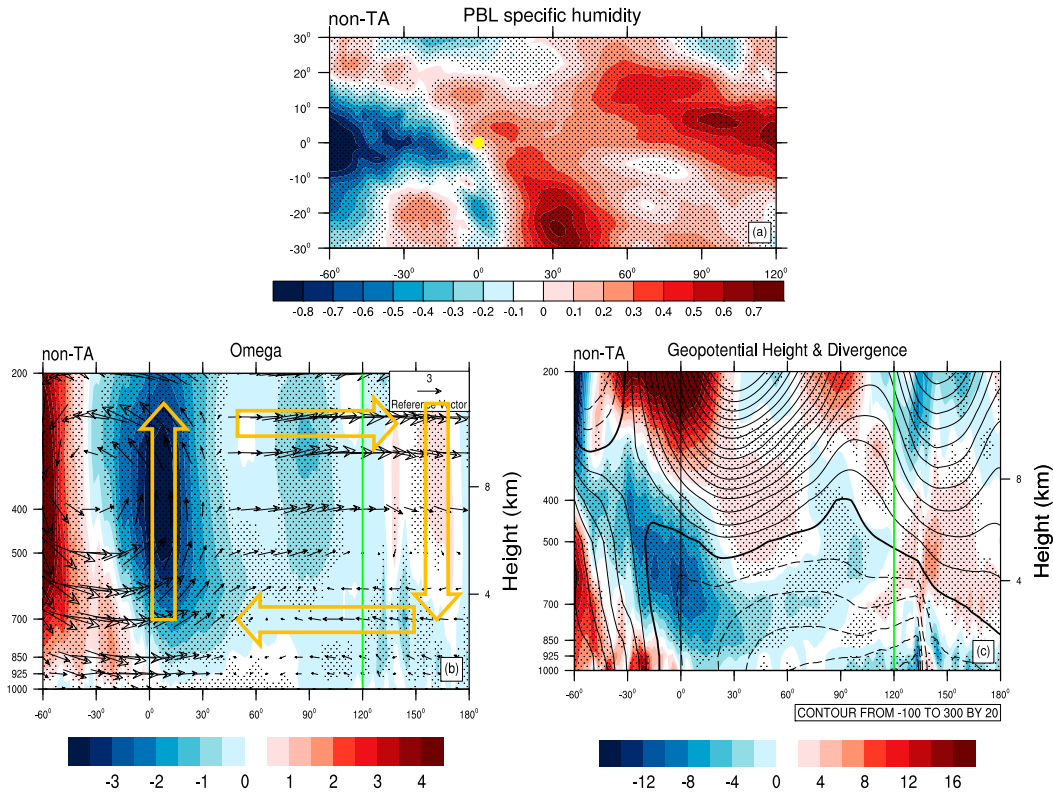
FIG. 7. (a)–(c) As in Figs. 2a, 2c, and 2d, but for the non-TA composite. A greater zonal domain is shown in (b) and (c) to reveal a wider anomalous vertical overturning circulation in the non-TA composite.

the central and eastern Pacific in group 3. As a result, the background precipitation distribution shifts westward.

The modulation of the background mean precipitation on an anomalous Gill response was discussed by various previous studies (e.g., Wu et al. 2009, 2017; Wang et al. 2017). According to Gill (1980), a positive heating anomaly associated with MJO convection can generate an anomalous vertical overturning circulation to its east as a result of Kelvin wave response. The so-generated descent motion to the east of the heating is in general weak and covers a wide region under a resting environment. However, the location of the anomalous descent is greatly modulated by the background mean precipitation due to the fact that a positive convection–circulation–moisture feedback happens in the mean precipitation region and that an anomalous descent cannot induce a negative rainfall anomaly in the mean subsidence region (Wu et al. 2009). As a result, the longitudinal location of the maximum descent depends greatly on the zonal distribution of the mean precipitation. The feedback-induced negative heating may further suppress the original anomalous overturning circulation to its east. In group 1, a strong descent anomaly appears at 70° (see the yellow downward arrow in Fig. 2c) due to the seasonal mean precipitation modulation. In groups 2 and 3, because the MJO center shifts eastward about 50° in longitude, the combined seasonal and interannual precipitation distribution becomes critical in modulating the anomalous vertical overturning circulation. An eastward shifting of the background precipitation associated

with an El Niño–like condition favors a similar mean precipitation modulation scenario in group 2, whereas a westward shifting of the background precipitation during a La Niña–like condition suppresses the aforementioned convection feedback in group 3. As a result, the anomalous response to MJO heating in group 3 is more like the original Gill solution, characterized by a weak but zonally expanded vertical overturning circulation.

To further validate the convection feedback argument above, we examine the MJO-scale OLR anomaly distribution in all the three groups. Figure 10 shows clearly that a positive OLR anomaly emerges in front of MJO convection in both groups 1 and 2. The positive OLR anomaly implies a negative heating anomaly, and its center is located at about 70°E of the MJO center, being in phase with the anomalous descent (Fig. 2c). In contrast, there is no obvious positive OLR anomaly in front of MJO convection in group 3. This confirms the non-feedback hypothesis discussed above. Because of the lack of feedback, a weak but more zonally expanded overturning circulation appears in group 3 (Fig. 7b).

The distinctive vertical velocity responses in the key analysis region (Figs. 5 and 8c) lead to a positive column-integrated MSE tendency in groups 1 and 2 but a negative column-integrated MSE tendency in group 3. Such a vertical overturning circulation difference in the free atmosphere, however, does not significantly affect the boundary layer moistening process (i.e., the MA mechanism). This is because Kelvin
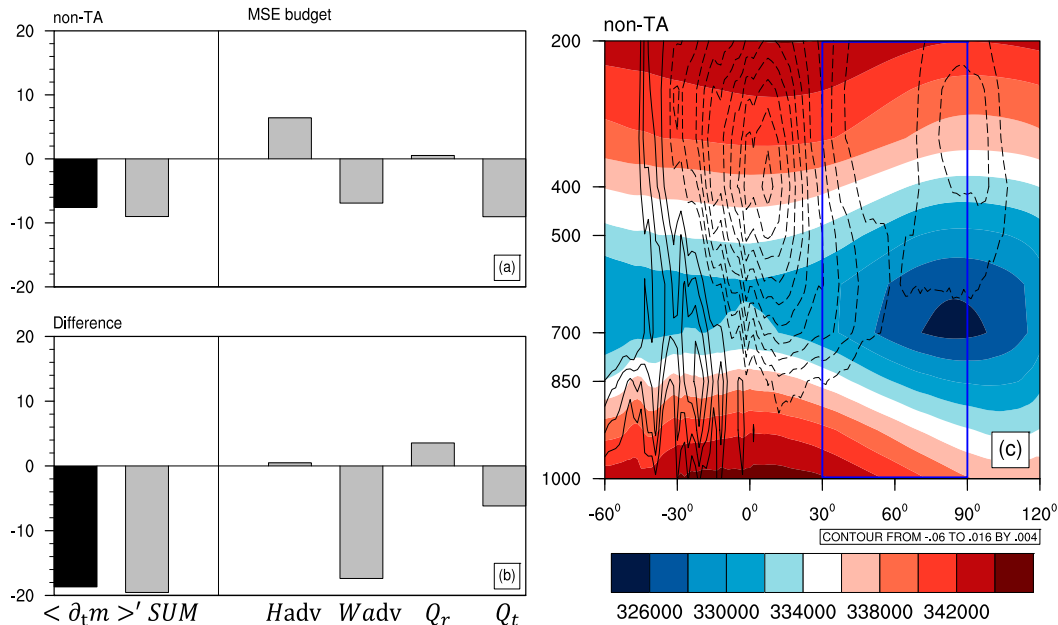
FIG. 8. Column-integrated MSE budget terms (kg s^{-3}) in the (a) non-TA composite averaged over the key region [blue box in (c)] and (b) difference between non-TA and total MJO days' right region average (gray bars in Fig. 3b). Bars from left to right represent, respectively, the MSE tendency, sum of budget terms, horizontal advection, vertical advection, radiation heating rate, and surface latent heat flux. (c) Vertical–zonal cross section of anomalously vertical velocity (contours; Pa s^{-1}) and mean MSE (m^2 s^{-2}) field. The blue box represents the key region.

wave–induced PBL convergence appears in all groups (Figs. 2d and 7c). For the MA mechanism, it is the lower-tropospheric easterly anomaly that plays the key role. In response to the MJO convective heating, Kelvin waves with low-level easterlies and low pressure appear to the east at the top of the PBL. This induces boundary layer convergence and upward motion. The mean moisture is then advected by the anomalous ascending motion. As a result, a positive moisture anomaly leads the convection. Figure 11 illustrates the zonal–vertical distribution of the anomalous specific humidity in the non-TA group. A clear vertically tilted moisture structure is seen, with positive boundary layer moisture anomalies leading the convection. According to the MA mechanism, the moisture leading can further induce convective instability east of MJO convection, promoting its eastward propagation.

A moisture budget over the boundary layer was further conducted to reveal the cause of the moisture leading in the non-TA group. Figure 12 shows that the main contribution arises from the vertical advection. A further diagnosis indicates that the positive vertical advection is primarily caused by the advection of the mean moisture by anomalous ascending motion. From Fig. 12, one can see that there is a low pressure anomaly in the front at the top of the PBL, which can induce anomalous boundary layer convergence there through the Ekman pumping process. Note that a negative SST anomaly appears in the boundary layer moistening region, suggesting that it is internal atmospheric process, not air–sea interaction, that contributes to the convergence.

To sum up, for the non-TA group, despite the negative MSE tendency in the front, the MJO continues to move eastward due to the MA mechanism. A positive PBL moisture anomaly appears to the east of MJO convection, due to the advection of the background mean moisture by anomalous ascending motion caused by the Kelvin wave–induced boundary layer convergence.

5. Summary and discussion

Recently, two types of the moisture mode theories have been proposed. The first type emphasizes the moisture asymmetry in the PBL (MA mechanism). It is argued that a positive boundary layer moisture anomaly in front of the convection can trigger convective instability and promotes the eastward propagation of the MJO. The second type emphasizes the column-integrated MSE tendency asymmetry (TA mechanism). It is argued that the MJO may be viewed as a column-integrated thermodynamic energy complex so that a zonally asymmetric MSE tendency with a positive anomaly to the east and a negative anomaly to the west can promote its eastward propagation. Under this theoretical framework, whether or not the PBL moisture is asymmetric is not critical. In this work, through a detailed diagnosis of the 33-yr observational data, we intend to validate the two popular moisture mode theories.

The RMM index is used to isolate the eastward-propagating MJO signal. A criterion is developed to retain strong, long-duration MJO events. A total of 2343 daily eastward
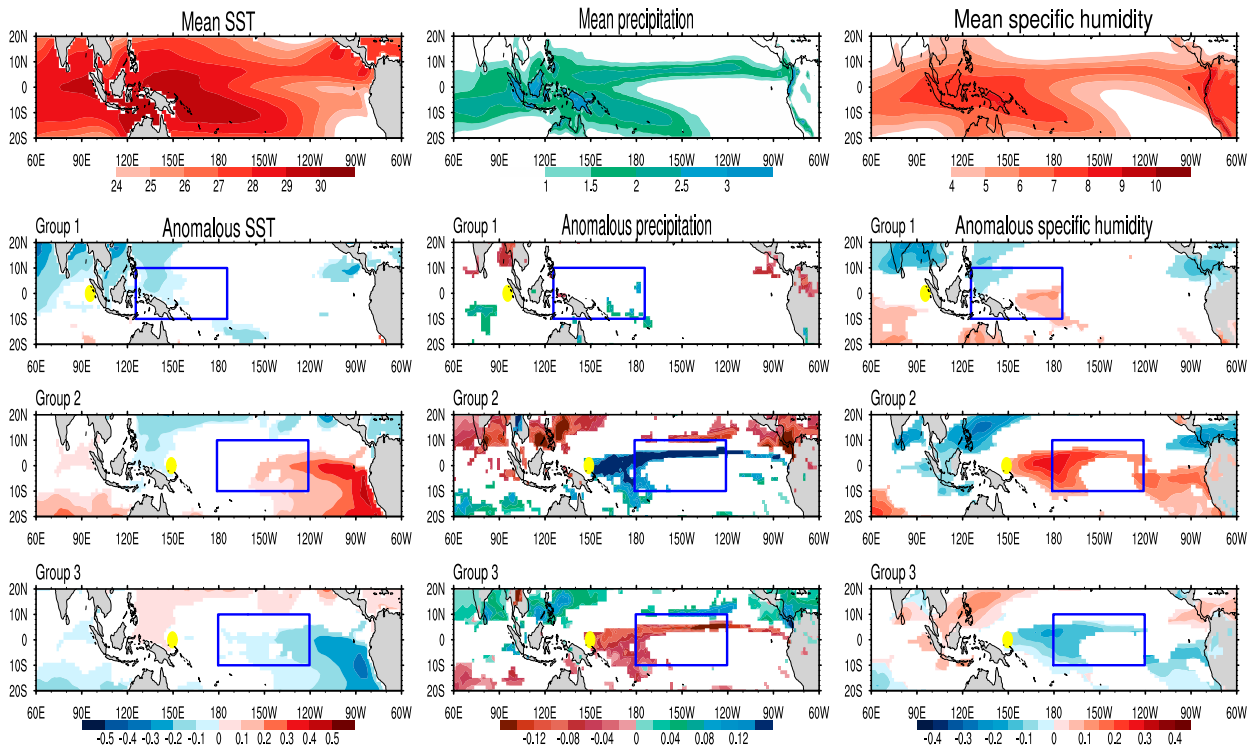
FIG. 9. (top) Patterns of the (left) mean SST (°C), (center) precipitation (mm day^{-1}), and (right) PBL specific humidity (g kg^{-1}). Patterns of anomalous SST, precipitation, and specific humidity fields for (second row) group 1 (MJO days west of 140°E), (third row) group 2 (MJO days east of 140°E with TA), and (bottom) group 3 (the non-TA group). Yellow dots denote the average MJO center at each group. Blue boxes represent the key analysis region (30°–90°) east of MJO center. Only areas exceeding a 95% confidence level are plotted for the lower panels.

propagating MJO days are selected for the 33 northern winter seasons. It is interesting to note that while all these MJO days show a clear PBL moisture leading, 80% of these days possess a clear positive column-integrated MSE tendency in front of the MJO convective center. The 20% remaining days have a negative MSE tendency in front of the convection, and they are all located east of 140°E.

Both the moisture asymmetry (MA) and the MSE tendency asymmetry (TA) mechanisms are well represented in the diagnosis of the all-day composite. For the former, a positive moisture anomaly occurs at the PBL to the east of MJO convection. The moisture anomaly arises primarily from the advection of the mean moisture by anomalous ascending motion, according to a moisture budget analysis. The anomalous ascent results from the MJO heating-induced Kelvin wave response and associated boundary layer convergence. For the latter, the positive MSE tendency in front of the convection arises from both the lower-tropospheric horizontal MSE advection and upper-tropospheric vertical MSE advection.

In contrast to the all-day composite, a negative MSE tendency appears in front of the MJO convection in the non-TA group. The cause of the difference lies in the zonal scale of the overturning circulation. While a descent appears in the key region in the total case composite (see Fig. 2c), a weaker ascent appears in the non-TA composite (see Fig. 7b). The former

induces a positive MSE tendency, whereas the latter induces a negative tendency. The vertical overturning circulation is still there, and the difference is attributed to the zonal extent of the circulation. By examining all the MJO days into three groups, days west of 140°E, days east of 140°E that satisfy the TA mechanism and the non-TA group, a background mean state modulation mechanism is proposed to explain the distinctive vertical velocity anomaly in front of MJO convection. Figure 13 is a schematic diagram that illustrates the modulation of the background mean state on the heating-induced anomalous vertical overturning circulation in front of the MJO convection. The location of the maximum descent in group 1 is primarily modulated by the seasonal mean precipitation, whereas in groups 2 and 3 it is modulated by the combined effect of the seasonal mean state and the ENSO-like patterns.

The mechanism through which the background precipitation modulates an anomalous Gill response is summarized as following. A positive heating anomaly associated with MJO convection can induce a Kelvin wave response with anomalous descent to its east (Gill 1980). The so-generated descent can only be amplified (through a positive convection–circulation–moisture feedback) when there is background mean precipitation. The process of this positive feedback can be summarized as following. In the region of the background convection, an
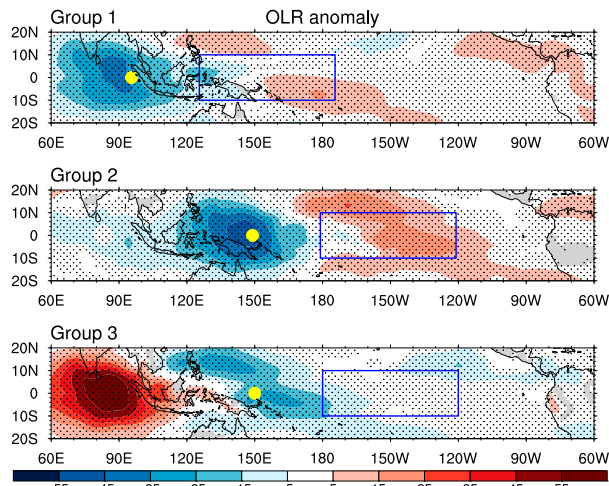
FIG. 10. Patterns of the MJO-scale OLR anomaly (W m^{-2}) for (top) group 1 (MJO days west of 140°E), (middle) group 2 (MJO days east of 140°E with TA), and (bottom) group 3 (the non-TA group). Yellow dots denote the average MJO center at each group. Blue boxes represent the key analysis region. Areas with dots exceed a 95% confidence level with Student's t test.

FIG. 11. Vertical–zonal cross section of specific humidity (g kg^{-1}) based on non-TA composite. The black line and box represent the MJO convective center and the key region, respectively.

anomalous descent reduces moisture through dry advection, leading to a negative heating anomaly in middle troposphere. The negative heating further decreases the thickness and induces a positive (negative) geopotential height anomaly in the lower (upper) troposphere, which promotes a low-level divergence and upper-level convergence. As a result, the anomalous descent is strengthened. Because of this positive feedback, the strength and longitudinal location of the anomalous descent associated with the Kelvin wave response depend greatly on the background precipitation distribution. For group 1, a strong descent appears in front of the convection due to the seasonal mean state modulation (Fig. 13a). For groups 2 and 3, because the mean MJO center shifts about 50° in longitude, the ENSO mode becomes critical in modulating the background state profile. An El Niño–like background condition in group 2 favors a strong but zonally more confined vertical overturning circulation (Fig. 13b). A La Niña–like background condition leads to a weak but zonally more expanded vertical overturning circulation (Fig. 13c), in a way similar to the original Gill response under a resting environment.

As stated in the introduction, the main objective of the current study is to validate the existing two moisture mode theories, based on the observational diagnosis. We confirm that both the moisture mode theories are in general operating in the real world. In particular, the two mechanisms work very well over the tropical Indian Ocean and the western Maritime Continent (west of 140°E). However, to the east of 140°E, it appears that only 23% of the MJO days support the TA mechanism, while 100% of these days support the MA mechanism.

The results above were obtained based on the filtered daily data. A parallel calculation was done with pentad data. The comparison of the two results shows no significant difference
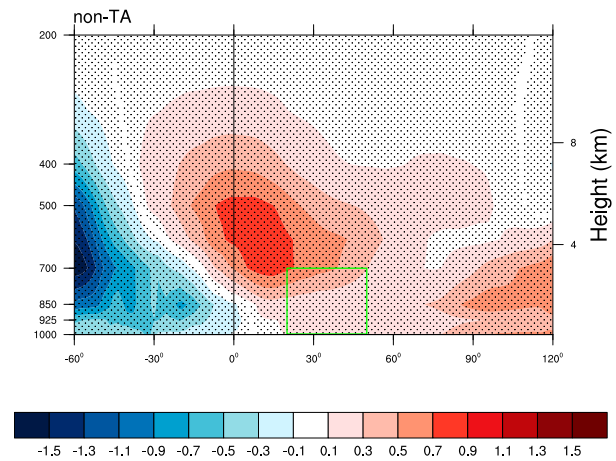
between the daily and pentad data results. Similarly, the sensitivity of the analysis result to the different domains of the TA and MA indices, for example enlarging the domain size by 50% and shifting zonally by 10° in longitude, has been examined. Results show that the main results are not sensitive to the domain change.

While the current study emphasizes the moisture mode theories, it is worth mentioning that MJO-like perturbations may be generated in a dry model without an explicit description of moisture (Yang and Ingersoll 2013, 2014). In the model, the convective available potential energy (CAPE) was used as a closure of cumulus parameterization. Even though some observed features of the MJO can be explained by the moisture mode theories, some weaknesses of the theories do exist (Pritchard and Yang 2016; Kacimi and Khouider 2018; Zhang et al. 2020). For example, there are several assumptions within the moisture mode theories, such as the precipitation being linearly proportional to the column moisture, no explicit description of the congestus (stratiform) cloud development in front (rear) of MJO convection, a nonjustified steady-state Gill response to the MJO heating (Kacimi and Khouider 2018), and the use of a too large damping coefficient in the free-atmospheric momentum and thermodynamic equations.

Caution is needed in interpreting the current analysis result because the reanalysis data contain biases. For example, Fu et al. (2011) noted that while the quality of the specific humidity field in ERA-Interim was better than that in NCEP I and II compared to satellite observations, all three reanalysis products underestimated the intensity of the eastward-propagating MJO. It is worth pointing out that the main objective of the current study is to validate the existing two moisture mode theories in terms of MJO propagation dynamics. Other important issues such as MJO planetary-scale selection and instability mechanisms are not examined. Through this effort, we intend to promote a deeper understanding and stimulate in-depth discussions of the current moisture mode theories. Further theoretical and observational
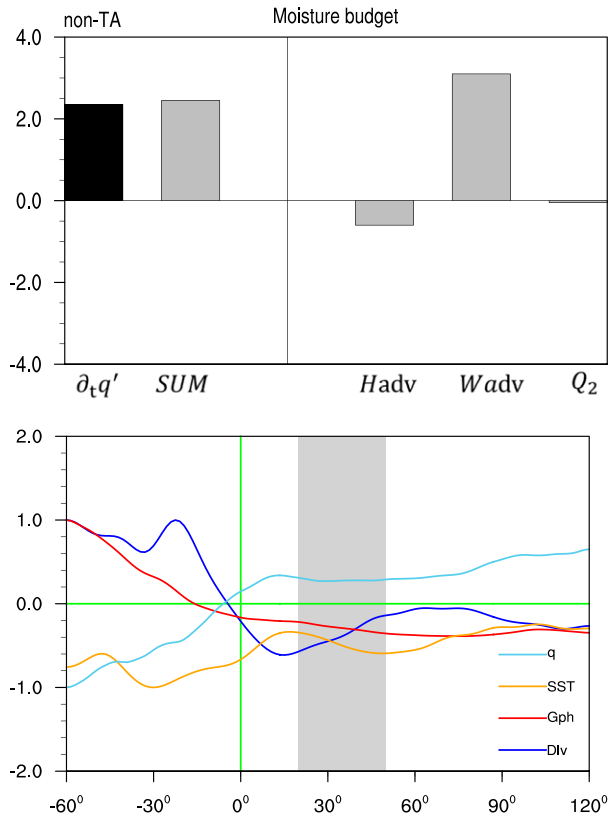
FIG. 12. (top) As in Fig. 3a and (bottom) as in Fig. 4, but for the non-TA composite and PBL specific humidity is normalized by $0.8 \, \text{g kg}^{-1}$.

studies are needed to understand the fundamental difference between the two moisture mode mechanisms and among different theories. While the current study focuses on the moisture mode theories, it is desirable to validate all existing theories using observational data including the WISHE (e.g., Emanuel 2020) and the multiscale interaction (e.g., Majda and Biello 2004) theories. An open question related to the moisture mode theories is what controls the MJO propagation speed. Is it controlled by the strength of the PBL moisture perturbation in front of the MJO convection, the column integrated MSE tendency asymmetry, or both? This issue will be discussed in the near future.

Data availability statement. Datasets are available in a public repository that assigns persistent identifiers to datasets.
1. Daily outgoing longwave radiation (OLR) used during this study are openly available from the European Center for
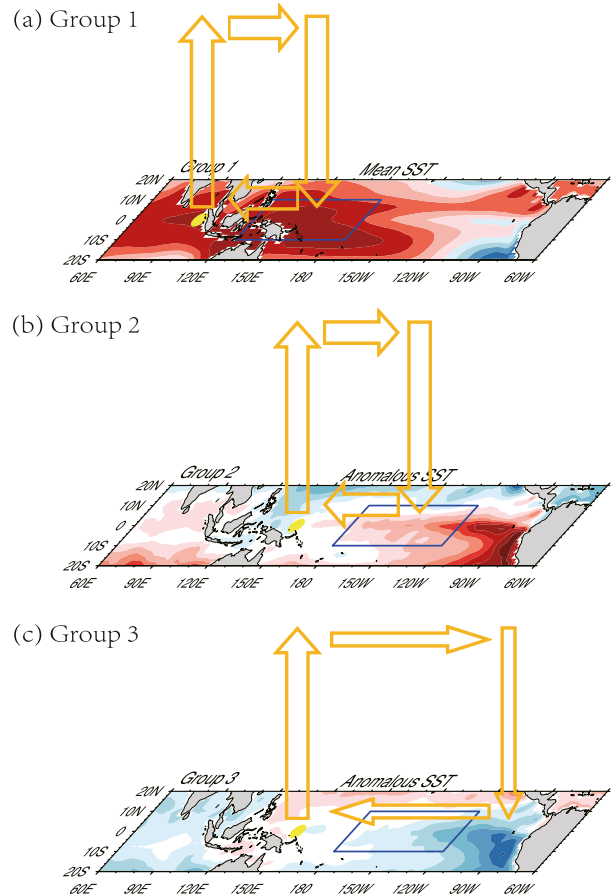

FIG. 13. Schematic diagram illustrating the heating-induced anomalous vertical overturning circulation (yellow arrows) for (a) group 1 (MJO days west of 140°E), (b) group 2 (MJO days east of 140°E with TA), and (c) group3 (MJO days east of 140°E with non-TA). A slightly narrow arrow indicates a weaker strength. The mean SST is shown in(a), whereas anomalous SST composites are shown in (b) and (c).

Medium-Range Weather Forecasts interim reanalysis (ERA-Interim) dataset at https://psl.noaa.gov/data/gridded/data.interp_OLR.html as cited in Liebmann and Smith (1996).
2. Daily reanalysis data consist of three-dimensional wind, geopotential height, temperature, specific humidity, and surface heat fluxes fields are openly available from the European Center for Medium-Range Weather Forecasts ERA-Interim dataset at https://rda.ucar.edu/datasets/ds627.0/ as cited in Dee et al. (2011).

REFERENCES

Adames, Á. F., and D. Kim, 2016: The MJO as a dispersive, convectively coupled moisture wave: Theory and observations. *J. Atmos. Sci.*, **73**, 913–941, https://doi.org/10.1175/JAS-D-15-0170.1.

Andersen, J. A., and Z. Kuang, 2012: Moist static energy budget of MJO-like disturbances in the atmosphere of a zonally symmetric aquaplanet. *J. Climate*, **25**, 2782–2804, https://doi.org/10.1175/JCLI-D-11-00168.1.

Biello, J. A., and A. J. Majda, 2005: A new multiscale model for the Madden–Julian oscillation. *J. Atmos. Sci.*, **62**, 1694–1721, https://doi.org/10.1175/JAS3455.1.

Chang, C.-P., and H. Lim, 1988: Kelvin wave-CISK: A possible mechanism for the 30–50 day oscillations. *J. Atmos. Sci.*, **45**, 1709–1720, https://doi.org/10.1175/1520-0469(1988)045<1709:KWCAPM>2.0.CO;2.

Dee, D. P., and Coauthors, 2011: The ERA-Interim reanalysis: Configuration and performance of the data assimilation system. *Quart. J. Roy. Meteor. Soc.*, **137**, 553–597, https://doi.org/10.1002/qj.828.

Del Genio, A. D., Y. Chen, D. Kim, and M.-S. Yao, 2012: The MJO transition from shallow to deep convection in CloudSat/CALIPSO data and GISS GCM simulations. *J. Climate*, **25**, 3755–3770, https://doi.org/10.1175/JCLI-D-11-00384.1.

Emanuel, K. A., 1987: An air–sea interaction model of intraseasonal oscillations in the tropics. *J. Atmos. Sci.*, **44**, 2324–2340, https://doi.org/10.1175/1520-0469(1987)044<2324:AASIMO>2.0.CO;2.

——, 2020: Slow modes of the equatorial waveguide. *J. Atmos. Sci.*, **77**, 1575–1582, https://doi.org/10.1175/JAS-D-19-0281.1.

Fu, X., B. Wang, J. Y. Lee, W. Wang, and L. Gao, 2011: Sensitivity of dynamical intraseasonal prediction skills to different initial conditions. *Mon. Wea. Rev.*, **139**, 2572–2592, https://doi.org/10.1175/2011MWR3584.1.

Gill, A. E., 1980: Some simple solutions for heat-induced tropical circulation. *Quart. J. Roy. Meteor. Soc.*, **106**, 447–462, https://doi.org/10.1002/qj.49710644905.

Hendon, H. H., and M. L. Salby, 1994: The life cycle of the Madden–Julian oscillation. *J. Atmos. Sci.*, **51**, 2225–2237, https://doi.org/10.1175/1520-0469(1994)051<2225:TLCOTM>2.0.CO;2.

Hsu, P.-C., and T. Li, 2012: Role of the boundary layer moisture asymmetry in causing the eastward propagation of the Madden–Julian oscillation. *J. Climate*, **25**, 4914–4931, https://doi.org/10.1175/JCLI-D-11-00310.1.

——, ——, L. You, J. Gao, and H. Ren, 2014: A spatial-temporal projection model for 10–30 day rainfall forecast in South China. *Climate Dyn.*, **44**, 1227–1244, https://doi.org/10.1007/s00382-014-2215-4.

Jiang, X., and Coauthors, 2015: Vertical structure and physical processes of the Madden–Julian oscillation: Exploring key model physics in climate simulations. *J. Geophys. Res. Atmos.*, **120**, 4718–4748, https://doi.org/10.1002/2014JD022375.

——, and Coauthors, 2020: Fifty years of research on the Madden–Julian oscillation: Recent progress, challenges, and perspectives. *J. Geophys. Res. Atmos.*, **125**, e2019JD030911, https://doi.org/10.1029/2019JD030911.

Johnson, R. H., and P. E. Ciesielski, 2013: Structure and properties of Madden–Julian oscillations deduced from DYNAMO sounding arrays. *J. Atmos. Sci.*, **70**, 3157–3179, https://doi.org/10.1175/JAS-D-13-065.1.

——, T. M. Rickenbach, S. A. Rutledge, P. E. Ciesielski, and W. H. Schubert, 1999: Trimodal characteristics of tropical convection. *J. Climate*, **12**, 2397–2418, https://doi.org/10.1175/1520-0442(1999)012<2397:TCOTC>2.0.CO;2.

Kacimi, A., and B. Khouider, 2018: The transient response to an equatorial heat source and its convergence to steady state: Implications for MJO theory. *Climate Dyn.*, **50**, 3315–3330, https://doi.org/10.1007/s00382-017-3807-6.

Khouider, B., and A. J. Majda, 2008: Multicloud models for organized tropical convection: Enhanced congestus heating. *J. Atmos. Sci.*, **65**, 895–914, https://doi.org/10.1175/2007JAS2408.1.

Kikuchi, K., and Y. N. Takayabu, 2004: The development of organized convection associated with the MJO during TOGA COARE IOP: Trimodal characteristics. *Geophys. Res. Lett.*, **31**, L10101, https://doi.org/10.1029/2004GL019601.

Kim, D., and E. D. Maloney, 2017: Simulation of the Madden–Julian oscillation using general circulation models. *The Global Monsoon System: Research and Forecast*, World Scientific, 119–130.

——, J. S. Kug, and A. H. Sobel, 2014: Propagating versus nonpropagating Madden–Julian oscillation events. *J. Climate*, **27**, 111–125, https://doi.org/10.1175/JCLI-D-13-00084.1.

Knutson, T. R., 1986: Global-scale intraseasonal oscillations of outgoing longwave radiation and 250 mb zonal wind during Northern Hemisphere summer. *Mon. Wea. Rev.*, **114**, 605–623, https://doi.org/10.1175/1520-0493(1986)114<0605:GSIOOO>2.0.CO;2.

Lau, K.-M., and P. H. Chan, 1986: Aspects of the 40–50 day oscillation during the northern summer as inferred from outgoing longwave radiation. *Mon. Wea. Rev.*, **114**, 1354–1367, https://doi.org/10.1175/1520-0493(1986)114<1354:AOTDOD>2.0.CO;2.

——, and L. Peng, 1987: Origin of low-frequency (intraseasonal) oscillations in the tropical atmosphere. Part I: Basic theory. *J. Atmos. Sci.*, **44**, 950–972, https://doi.org/10.1175/1520-0469(1987)044<0950:OOLFOI>2.0.CO;2.

Lau, N.-C., and K.-M. Lau, 2010: The structure and propagation of intraseasonal oscillations appearing in a GFDL general circulation model. *J. Atmos. Sci.*, **43**, 2023–2047, https://doi.org/10.1175/1520-0469(1986)043<2023:TSAPOI>2.0.CO;2.

Li, T., 2014: Recent advance in understanding the dynamics of the Madden–Julian oscillation. *J. Meteor. Res.*, **28**, 1–33, https://doi.org/10.1007/s13351-014-3087-6.

——, and B. Wang, 1994: The influence of sea surface temperature on the tropical intraseasonal oscillation: A numerical study. *Mon. Wea. Rev.*, **122**, 2349–2362, https://doi.org/10.1175/1520-0493(1994)122<2349:TIOSST>2.0.CO;2.

——, and C. Zhou, 2009: Planetary scale selection of the Madden–Julian oscillation. *J. Atmos. Sci.*, **66**, 2429–2443, https://doi.org/10.1175/2009JAS2968.1.

——, and P.-C. Hsu, 2017: *Fundamentals of Tropical Climate Dynamics*. Springer, 229 pp.

——, and F. Hu, 2019: A coupled moisture-dynamics model of the Madden–Julian oscillation: Convection interaction with first and second baroclinic modes and planetary boundary layer. *Climate Dyn.*, **53**, 5529–5546, https://doi.org/10.1007/s00382-019-04879-x.

——, L. Wang, M. Peng, B. Wang, C. Zhang, W. Lau, and H.-C. Kuo, 2018: A paper on the tropical intraseasonal oscillation published in 1963 in a Chinese journal. *Bull. Amer. Meteor. Soc.*, **99**, 1765–1779, https://doi.org/10.1175/BAMS-D-17-0216.1.

——, J. Ling, and P. Hsu, 2020: Madden–Julian oscillation: Its discovery, dynamics, and impact on East Asia. *J. Meteor. Res.*, **34**, 20–42, https://doi.org/10.1007/s13351-020-9153-3.

Liebmann, B., and C. A. Smith, 1996: Description of a complete (interpolated) outgoing longwave radiation dataset. *Bull. Amer. Meteor. Soc.*, **77**, 1275–1277, https://www.jstor.org/stable/26233278.

Lindzen, R. S., and S. Nigam, 1987: On the role of sea surface temperature gradients in forcing low-level winds and convergence in the tropics. *J. Atmos. Sci.*, **44**, 2418–2436, https://doi.org/10.1175/1520-0469(1987)044<2418:OTROSS>2.0.CO;2.

Madden, R. A., and P. R. Julian, 1971: Detection of a 40–50 day oscillation in the zonal wind in the tropical Pacific. *J. Atmos. Sci.*, **28**, 702–708, https://doi.org/10.1175/1520-0469(1971)028<0702:DOADOI>2.0.CO;2.

——, and ——, 1972: Description of global-scale circulation cells in the tropics with a 40–50 day period. *J. Atmos. Sci.*, **29**, 1109–1123, https://doi.org/10.1175/1520-0469(1972)029<1109:DOGSCC>2.0.CO;2.

Majda, A. J., and J. A. Biello, 2004: A multiscale model for tropical intraseasonal oscillations. *Proc. Natl. Acad. Sci. USA*, **101**, 4736–4741, https://doi.org/10.1073/pnas.0401034101.

——, and S. N. Stechmann, 2009: The skeleton of tropical intra-seasonal oscillations. *Proc. Natl. Acad. Sci. USA*, **106**, 8417–8422, https://doi.org/10.1073/pnas.0903367106.

Maloney, E. D., 2009: The moist static energy budget of a composite tropical intraseasonal oscillation in a climate model. *J. Climate*, **22**, 711–729, https://doi.org/10.1175/2008JCLI2542.1.

——, Á. F. Adames, and H. X. Bui, 2019: Madden–Julian oscillation changes under anthropogenic warming. *Nat. Climate Change*, **9**, 26–33, https://doi.org/10.1038/s41558-018-0331-6.

Matsuno, T., 1966: Quasi-geostrophic motions in the equatorial area. *J. Meteor. Soc. Japan*, **44**, 25–43, https://doi.org/10.2151/jmsj1965.44.1_25.

Neelin, J. D., and I. M. Held, 1987: Modeling tropical convergence based on the moist static energy budget. *Mon. Wea. Rev.*, **115**, 3–12, https://doi.org/10.1175/1520-0493(1987)115<0003:MTCBOT>2.0.CO;2.

Pritchard, M. S., and D. Yang, 2016: Response of the super-parameterized Madden–Julian oscillation to extreme climate and basic-state variation challenges a moisture mode view. *J. Climate*, **29**, 4995–5008, https://doi.org/10.1175/JCLI-D-15-0790.1.

Sobel, A., and E. Maloney, 2012: An idealized semi-empirical frame-work for modeling the Madden–Julian oscillation. *J. Atmos. Sci.*, **69**, 1691–1705, https://doi.org/10.1175/JAS-D-11-0118.1.

——, and ——, 2013: Moisture modes and the eastward propaga-tion of the MJO. *J. Atmos. Sci.*, **70**, 187–192, https://doi.org/10.1175/JAS-D-12-0189.1.

Sperber, K. R., 2003: Propagation and the vertical structure of the Madden–Julian oscillation. *Mon. Wea. Rev.*, **131**, 3018–3037, https://doi.org/10.1175/1520-0493(2003)131<3018:PATVSO>2.0.CO;2.

Thual, S., and A. J. Majda, 2015: A suite of skeleton models for the MJO with refined vertical structure. *Math. Climate Wea. Forecasting*, **1**, 70–95, https://doi.org/10.1515/mcwf-2015-0004.

——, and ——, 2016: A skeleton model for the MJO with refined vertical structure. *Climate Dyn.*, **46**, 2773–2786, https://doi.org/10.1007/s00382-015-2731-x.

——, ——, and S. N. Stechmann, 2014: A stochastic skeleton model for the MJO. *J. Atmos. Sci.*, **71**, 697–715, https://doi.org/10.1175/JAS-D-13-0186.1.

Wang, B., 1988a: Comments on "An air–sea interaction model of intraseasonal oscillation in the tropics." *J. Atmos. Sci.*, **45**, 3521–3525, https://doi.org/10.1175/1520-0469(1988)045<3521:COAIMO>2.0.CO;2.

——, 1988b: Dynamics of tropical low-frequency waves: An analysis of the moist Kelvin wave. *J. Atmos. Sci.*, **45**, 2051–2065, https://doi.org/10.1175/1520-0469(1988)045<2051:DOTLFW>2.0.CO;2.

——, and H. Rui, 1990: Dynamics of the coupled moist Kelvin–Rossby wave on an equatorial β-plane. *J. Atmos. Sci.*, **47**, 397–413, https://doi.org/10.1175/1520-0469(1990)047<0397:DOTCMK>2.0.CO;2.

——, and T. Li, 1993: A simple tropical atmosphere model of relevance to short-term climate variations. *J. Atmos. Sci.*, **50**, 260–284, https://doi.org/10.1175/1520-0469(1993)050<0260:ASTAMO>2.0.CO;2.

——, and ——, 1994: Convective interaction with boundary-layer dynamics in the development of a tropical intraseasonal sys-tem. *J. Atmos. Sci.*, **51**, 1386–1400, https://doi.org/10.1175/1520-0469(1994)051<1386:CIWBLD>2.0.CO;2.

——, and G. Chen, 2017: A general theoretical framework for under-standing essential dynamics of Madden–Julian oscillation. *Climate Dyn.*, **49**, 2309–2328, https://doi.org/10.1007/s00382-016-3448-1.

——, F. Liu, and G. Chen, 2016: A trio-interaction theory for Madden–Julian oscillation. *Geosci. Lett.*, **3**, 34, https://doi.org/10.1186/s40562-016-0066-z.

——, and Coauthors, 2018: Dynamics-oriented diagnostics for the Madden–Julian oscillation. *J. Climate*, **31**, 3117–3135, https://doi.org/10.1175/JCLI-D-17-0332.1.

Wang, L., and T. Li, 2020a: Reexamining the MJO moisture mode theories with normalized phase evolutions. *J. Climate*, **33**, 8523–8536, https://doi.org/10.1175/JCLI-D-20-0202.1.

——, and ——, 2020b: Effect of vertical moist static energy ad-vection on MJO eastward propagation: Sensitivity to analysis domain. *Climate Dyn.*, **54**, 2029–2039, https://doi.org/10.1007/s00382-019-05101-8.

——, ——, E. Maloney, and B. Wang, 2017: Fundamental causes of propagating and non-propagating MJOs in MJOTF/GASS models. *J. Climate*, **30**, 3743–3769, https://doi.org/10.1175/JCLI-D-16-0765.1.

——, ——, and T. Nasuno, 2018: Impact of Rossby and Kelvin wave components on MJO eastward propagation. *J. Climate*, **31**, 6913–6931, https://doi.org/10.1175/JCLI-D-17-0749.1.

Wheeler, M. C., and H. H. Hendon, 2004: An all-season real-time multivariate MJO index: Development of an index for monitoring and prediction. *Mon. Wea. Rev.*, **132**, 1917–1932, https://doi.org/10.1175/1520-0493(2004)132<1917:AARMMI>2.0.CO;2.

Wu, B., T. Zhou, and T. Li, 2009: Contrast of rainfall–SST rela-tionships in the western North Pacific between the ENSO-developing and ENSO-decaying summers. *J. Climate*, **22**, 4398–4405, https://doi.org/10.1175/2009JCLI2648.1.

——, ——, and ——, 2017: Atmospheric dynamic and thermody-namic processes driving the western North Pacific anomalous anticyclone during El Niño. Part II: Formation processes. *J. Climate*, **30**, 9637–9650, https://doi.org/10.1175/JCLI-D-16-0495.1.

Xiang, B., M. Zhao, X. Jiang, S.-J. Lin, T. Li, X. Fu, and G. Vecchi, 2015: The 3–4-week MJO prediction skill in a GFDL coupled model. *J. Climate*, **28**, 5351–5364, https://doi.org/10.1175/JCLI-D-15-0102.1.

Xie, Y.-B., S.-J. Chen, I.-L. Zhang, and Y.-L. Hung, 1963: A pre-liminarily statistic and synoptic study about the basic currents over southeastern Asia and the initiation of typhoon (in Chinese). *Acta Meteor. Sin.*, **33**, 206–217.

Yanai, M., S. Esbensen, and J. H. Chu, 1973: Determination of bulk properties of tropical cloud clusters from large-scale heat and moisture budgets. *J. Atmos. Sci.*, **30**, 611–627, https://doi.org/10.1175/1520-0469(1973)030<0611:DOBPOT>2.0.CO;2.

Yang, D., and A. P. Ingersoll, 2013: Triggered convection, gravity waves, and the MJO: A shallow-water model. *J. Atmos. Sci.*, **70**, 2476–2486, https://doi.org/10.1175/JAS-D-12-0255.1.

——, and ——, 2014: A theory of the MJO horizontal scale. *Geophys. Res. Lett.*, **41**, 1059–1064, https://doi.org/10.1002/2013GL058542.

Zhang, C., 2005: Madden–Julian oscillation. *Rev. Geophys.*, **43**, RG2003, https://doi.org/10.1029/2004RG000158.

——, Á. F. Adames, B. Khouider, B. Wang, and D. Yang, 2020: Four theories of the Madden–Julian oscillation. *Rev. Geophys.*, **58**, e2019RG000685, https://doi.org/10.1029/2019RG000685.

Zhu, Z. W., T. Li, P. C. Hsu, and J. H. He, 2015: A spatial-temporal projection model for extended-range forecast in the tropics. *Climate Dyn.*, **45**, 1085–1098, https://doi.org/10.1007/s00382-014-2353-8.